Morphodynamic impacts of large-scale engineering projects in the Yangtze River delta

Luan, Hualong; Ding, P; Wang, Zhengbing ; Yang, S.L.; Lu, Jin You

DOI
10.1016/j.coastaleng.2018.08.013

Publication date
2018

Document Version
Final published version

Published in
Coastal Engineering

Coastal Engineering 141 (2018) 1–11

Contents lists available at ScienceDirect

Coastal Engineering

journal homepage: www.elsevier.com/locate/coastaleng

Morphodynamic impacts of large-scale engineering projects in the Yangtze River delta

Hua Long Luan[a,b], Ping Xing Ding[b,*], Zheng Bing Wang[b,c,d], Shi Lun Yang[b], Jin You Lu[a]

[a] Changjiang River Scientific Research Institute, Wuhan 430010, China
[b] State Key Laboratory of Estuarine and Coastal Research, East China Normal University, Shanghai 200062, China
[c] Faculty of Civil Engineering and Geosciences, Delft University of Technology, P.O. Box 5048, 2600 GA Delft, The Netherlands
[d] Deltares, P.O. Box 177, 2600 MH Delft, The Netherlands

ARTICLE INFO

Keywords:
Morphodynamics
Estuarine engineering projects
Process-based modeling
Yangtze river delta

ABSTRACT

Morphodynamics of world's river deltas are increasingly affected by human activities, which are of great ecological, economic and social implications. However, impacts of human interventions in deltaic regions are insufficiently understood, especially superimposed upon diminishing sediment supplies. This study uses the heavily interfered Yangtze River delta as an example to address this issue. The morphodynamic impacts of the Deepwater Navigation Channel Project (DNCP) during 1997–2013 are investigated through process-based modeling approach (Delft3D) and bathymetric data analysis. The DNCP was implemented in the mouth bar area of the Yangtze River delta including the twin dikes and 19 groynes with the total length of 132.0 km. Hydrodynamic simulations indicate that the training walls resulted in weaker tidal flow and longer slack period at the East Hengsha Shoal (EHS) and stronger tidal flow at the subaqueous delta. Thus, the EHS is characterized as a sediment accumulation zone after the completion of the training walls. Subsequently, morphological modeling shows enhanced accretion at the EHS and enhanced erosion at the subaqueous delta when the training walls are taken into account. Numerical experiments further demonstrate that the above changes are mainly attributed to the seaward half of the northern training walls constructed in 2002–2005. This is probably the reason for the observed accretion peak of the EHS in 2002–2007 and the gradual increase in the erosion rate of the subaqueous delta after 2002. The schematized paths of sediment transport after the DNCP indicate that sediment eroded from the subaqueous delta serves as an important source for accretion of the mouth bar area. It is suggested that siltation promoting projects within the mouth bar area increased shallow shoal accretion and aggravated erosion at the subaqueous delta. With the overall erosion of the Yangtze River delta due to river sediment reduction, large-scale estuarine engineering projects substantially increase the complicacy of its morphodynamic pattern, which merits close attention for sustainable delta management.

1. Introduction

Modern deltas across the globe, originated since the maximum Holocene transgression (Stanley and Warne, 1994), are actively propagating systems as redundant fluvial sediment accumulated hereon after part of the amount being taken away by marine currents (Coleman and Wright, 1975; Galloway, 1975). The progradation processes are increasingly interfered by human activities in drainage basins throughout the past century, and many of world's largest deltas are at risk of or currently suffering from erosion and flooding as a result of sediment trapping in upstream reservoirs in combination with relative sea-level rise (Syvitski et al., 2009). Meanwhile, engineering controls within deltaic regions induce rapid and significant changes at adjacent areas, and may complicate the overall evolution patterns overlying upstream human interventions. A regime shift from natural evolution driven to anthropogenic impact driven is likely to occur in terms of deltaic morphodynamics (Syvitski and Saito, 2007). Protecting these dynamic and vulnerable environments from deterioration is an issue of global concern, regarding that river deltas are home to more than half a billion people and thousands of plant and animal species, and thereby hold high ecological and socio-economic values (Day et al., 1989).

The close link between human-induced decrease of sediment loads and delta erosion has been identified by numerous case studies on large deltas, including the Nile (Stanley, 1996), Mississippi (Blum and Roberts, 2009), Ebro (Sanchez-Arcilla et al., 1998), Mekong (Anthony et al., 2015), and Yellow River (Chu et al., 2006; Wang et al., 2007).

* Corresponding author.
E-mail address: pxding@sklec.ecnu.edu.cn (P.X. Ding).

https://doi.org/10.1016/j.coastaleng.2018.08.013
Received 9 March 2018; Received in revised form 29 June 2018; Accepted 21 August 2018
Available online 22 August 2018
0378-3839/

Most densely populated deltas were further interfered by vicinal human interventions. The Mississippi River Delta, for instance, is suffering from rapid subsidence and land loss caused by intensive hydrocarbon extraction (Morton et al., 2005). The Eastern Scheldt estuary showed overall erosion at the ebb-tidal delta and tidal flats within the estuary after the construction of the storm surge barrier in 1986 (Eelkema et al., 2013; Wang et al., 2015; de Vet et al., 2017). Flow path control of distributary channels created new delta surface as occurred in the deltas of the Yellow River, Colorado River and Po River (Syvitski and Saito, 2007). The tide-dominant Mersey Estuary (UK) experienced significant accretion in 1906–1977 due to the construction of training walls and dredging activity (Thomas et al., 2002). Local human interventions, including training wall construction, dredging and land reclamation, can induce either severe accretion or intensive deepening in deltaic areas (Blott et al., 2006; Wu et al., 2016). Rapid urbanization and resource utilization within deltaic areas are likely to aggravate the risk and sustainability of river deltas, compounded with river sediment reduction and rising seas (Syvitski, 2008). Identifying the distinct morphological impacts of local human activities can strengthen our understanding on delta evolution processes and future trends, and provide guidance for integrated delta management.

The large-scale and densely populated Yangtze River delta in China provides a unique example to examine deltaic morphodynamics in response to human interventions from both the upstream reach and deltaic region (Fig. 1) (De Vriend et al., 2011). Under decreasing river sediment supply after the constructions of more than 50,000 dams throughout the watershed (Yang et al., 2011), multiple evidences for delta erosion have been identified in terms of bed level changes (Yang et al., 2011), grain size variations (Luo et al., 2017; Yang et al., 2018), sediment transport capacity of coastal currents (Deng et al., 2017), magnetic methods (Ge et al., 2017) and isotopic tracing (Wang et al., 2017). However, the Yangtze River delta showed complicated evolution pattern in recent years, which cannot be merely explained by fluvial sediment reduction. Luan et al. (2016) found that the northern part of the mouth bar area converted from net erosion in 1986–1997 to net accretion in 1997–2010, and the mouth bar area in the latter period retained net accretion with erosion in its southern subaqueous delta. Hydrodynamic simulations by Zhu et al. (2016) indicated that the recent erosion of the subaqueous delta can be related to the training walls constructed along the North Passage. The training walls also contributed to accretion and seaward elongation of the adjacent Jiuduansha Shoal (Li et al., 2016; Wei et al., 2016). Previous studies examined morphological changes of the mouth bar area before and after the constructions of training walls, whereas shorter-term evolution processes within the period (1997–2010) and their physical mechanisms were poorly revealed.

Many estuarine engineering projects have been constructed within the estuary in the recent two decades for navigation, flood control, freshwater consumption and wetland management purposes (Tian et al., 2015; Luan et al., 2016). The separated impacts of local human interventions and river sediment reduction on morphological changes of the Yangtze River delta are still less understood, which is the main motivation underlying the present study. The study area is defined as the seaward part of mouth bar area and adjacent subaqueous delta, spanning from the East Hengsha Shoal (EHS) and Jiuduansha Shoal (JS) to the isobath of nearly 30 m (Fig. 1b). Morphological processes are quantified based on bathymetric data of multiple years during 1997–2013. Considering the complexity of evolution pattern of the study area, the process-based modeling approach (Delft3D) is applied to investigate the morphological impacts and relevant mechanisms of large-scale estuarine engineering projects since 1997. The results should be valuable for sustainable management of the Yangtze River delta and other densely populated large river deltas in the world.

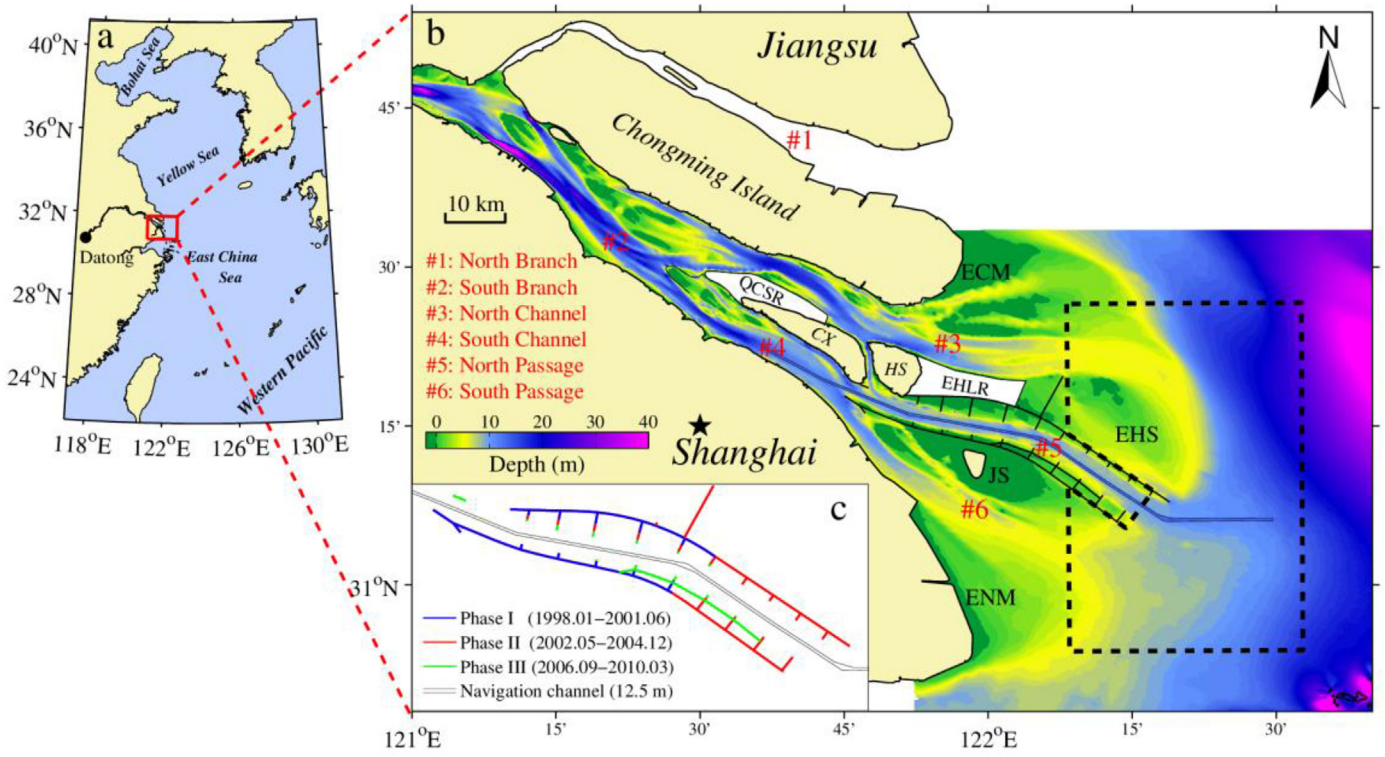

Fig. 1. (a) The location of the Yangtze Estuary on the western coast of the East China Sea (rectangle); (b) the Yangtze Estuary with bathymetry observed in 2010; (c) training walls constructed in three phases during 1997–2010. The dashed lines in (b) denote the boundary of the study area. ECM: East Chongming Mudflat; EHS: East Hengsha Shoal; JS: Jiuduansha Shoal; ENM: East Nanhui Mudflat; CX: Changxing Island; HS: Hengsha Island; QCSR: Qingcaosha Reservoir; and EHLR: East Hengsha Land Reclamation.

2. Study area

The Yangtze River, ranking the largest and longest in Asia (Milliman and Farnsworth, 2011), reaches its end near Shanghai City and enters the inner shelf of the East China Sea (Fig. 1a). The Yangtze River delta receives huge amount of river inputs from the upstream watershed, i.e. 893 km^3/yr of runoff and 368 Mt/yr of suspended sediment load in 1950–2015. Mean tidal range and wave height at the mouth is 2.67 m and 0.9 m, respectively (Yun, 2004). Under combined large river flow, meso-tidal and minor wave forcing, the Yangtze River delta is defined as a mixed river- and tidal-dominant delta and featured by a funnel-shaped topography with wide distributary channels and accreting intertidal flats in a long-term (Fig. 1b). No significant variation trend was observed for the annual water runoff in the past half century, while the annual sediment load decreased continuously after the 1980s. The sediment load dropped to a relatively low level in the first decade after the closure of the Three Gorge Dam (2003–2013, 143 Mt/yr) which is only about 30% of that in 1950–1968 (Yang et al., 2015). Notably, the sediment load was as low as 85 Mt/yr and 72 Mt/yr in the extreme drought year 2006 and 2011, respectively.

The Yangtze subaqueous delta covers an area of over 10,000 km^2 spanning from the mouth to the paleo-incised valley (30–50 m) (Chen et al., 1985). The seabed at the mouth bar area is dominated by cohesive mud which can be frequently resuspended by tidal currents (Liu et al., 2010; Luo et al., 2012). This area behaves as both the estuarine turbidity maximum and depocenter of the delta (Chen et al., 1985; Dai et al., 2014). In the recent two decades, many engineering projects have been constructed within the mouth bar area. One of the largest is the Deep Navigation Channel Project (DNCP) in the mouth bar area including training wall constructions and intensive dredging (Fig. 1b), which was aimed at improving the navigation. The DNCP was implemented through three phases from 1998 to 2010, i.e., Phase I (1998.01–2001.06), Phase II (2002.05–2004.12) and Phase III (2006.09–2010.03) (Fig. 1c). The present configuration of the twin dikes along both sides of the North Passage was completed in the Phase II, while the Phase III mainly includes groyne extensions, the partition dike in the south side and intensive dredging. The north and south dike are 49.2 km and 48.1 km long, respectively. The groynes are perpendicular to the proximal dike with ten on the north side and nine on the south side. The total length of the T-shaped groynes is 34.7 km. The height of these training walls is approximately 0.3 m relative to the mean sea-level, which means that they are emerged at low tide and submerged at high tide. A bidirectional deep navigation channel with the length 92.2 km and the width 350–400 m formed along the North Passage due to continuous dredging, and the depth of the navigation increased from 6.5 m before the project to 8.5 m in 2001, 10 m in 2005 and 12.5 m in 2011. Thus, the mouth bar in the North Passage was artificially broken through after a plenty of dredging efforts. The bathymetry within the North Passage responded rapidly to the construction of training walls, as reflected by severe deposition in the groyne-sheltered areas and back-siltation in the navigational channel (Liu et al., 2011; Dai et al., 2013). The DNCP is by far the largest estuarine engineering project in China whose morphological impacts have extended beyond their given sites (Luan et al., 2016). Other engineering projects within the deltaic region include the siltation promoting project and land reclamation at the EHS and the East Nanhui Mudflat. Some groins were constructed to weaken the regional flow intensity and induce shoal accretion (Wei et al., 2015).

3. Method

3.1. Process-based morphological modeling

The process-based Delft3D model system is applied to examine the impacts of training walls on hydrodynamics and morphological evolution. The model solves shallow water equations under hydrostatic pressure assumption in a horizontal curvilinear grid and is fully integrated with hydrodynamic, sediment transport and morphological updating modules (Lesser et al., 2004). Medium-to long-term morphodynamic modeling can be implemented through linearly accelerating bed-level change at each hydrodynamic time step with a carefully selected morphological factor (MF) (Roelvink, 2006). Thus, the model online couples flow and morphology simulation, and produces bathymetric change of a linearly up-scaled period. Numerous case studies have demonstrated high capacity of the Delft3D model system on reproducing detailed flow features, sediment dynamics and morphological evolution of coastal and estuarine environments (van der Wegen et al., 2011; Dissanayake et al., 2012; van Maren et al., 2015; Su et al., 2016; Luan et al., 2017).

The model domain covers the entire Yangtze Estuary ranging from the upstream tidal limit (Datong) to the outer sea. The grid size varies from ~300 m within the estuary to ~3 000 m near the offshore boundary, which is sufficient for simulating morphological behaviors of the Yangtze Estuary with acceptable accuracy. The time step of the hydrodynamic model is 2 min according to the CFL criteria. The training walls along the North Passage are represented in the model as Current Deflection Walls (CDW), which allow the water to flow over when the water level is sufficiently high (Deltares, 2014). Major physical driving forces are considered in the model including astronomic tides, river flow and wind wave. The offshore boundaries are driven by 8 main astronomic components (M2, S2, K1, O1, N2, K2, P1, and Q1) derived from a well-validated large model covering the East China Sea (Ge et al., 2013). Currents across the boundaries are calculated by the model. The tangential component of coastal currents is absent due to the unnecessary complexity in morphological modeling when prescribing both astronomic tides and coastal currents along the offshore boundaries (van der Wegen et al., 2011). Wave parameters are calculated by SWAN (http://www.swan.tudelft.nl) using monthly climatological wind data (1995–2005). The wave information obtained each hour is coupled with the flow and morphological model offline. River inputs are schematized in the model based on monthly-averaged water and sediment discharges. The values of MFs depending on the amplitude of water discharge are determined after sensitivity analysis. The model considers multiple sediment fractions (cohesive and non-cohesive), which are based on grain size and composition analysis of bed sediment samples in the estuarine area. More details about the model setup were described by Luan et al. (2017).

Promising hindcasting at a decadal timescale was carried out for three historical periods involving distinct morphological processes, i.e., a rapid accretion period (1958–1978), an erosional period (1986–1997) and a recent period with slight accretion (2002–2010). The hindcast case of the recent period, which corresponds to the constructing period of the DNCP, shows the best model performance, and thereby provides a nice reference case. One numerical experiment is firstly conducted which excludes all training walls along the North Passage from the reference case to explore the overall impacts of the DNCP. The twin dikes were extended to the present location after the Phase II of the DNCP and induced severe siltation in the middle of the dredged channel (Liu et al., 2011). Dikes and groynes implemented in the Phase II are close to the EHS and the observed erosion zones at the subaqueous delta (Luan et al., 2016; Zhu et al., 2016). Therefore, two further numerical experiments are conducted which exclude the seaward half of the northern and southern training walls from the reference case, respectively. The modeled hydrodynamics, sediment transport processes and subsequent bed-level changes in the above three experiments are compared with the reference case to provide physical explanation of the observed evolution under large-scale estuarine engineering projects.

3.2. Data collection and processing

To assess the morphological processes, we collected navigational charts and bathymetric maps for various years (1997, 2002, 2007, 2010

and 2013) which captured each phase of the DNCP. For the comparison purpose, bathymetric data in 1986 was also collected. For the bathymetry measurements, an echo sounder and a global positioning system (Trimble Navigation Limited, California, USA) were used for depth measurements and position recordings, respectively, with vertical and horizontal errors of 0.1 m and 1 m. The scales of the maps range from 1:50,000 to 1:130,000. The averaged data density is 3–13 samples/km^2, which is sufficiently high for calculating bathymetric changes greater than 0.1 m (Dai et al., 2014; Luo et al., 2017). Depth points of each year, referenced to the theoretical lowest-tide datum at Wusong, are interpolated into a 50 × 50 m grid by the Kriging interpolation technique in the Surfer mapping software package, generating a digital elevation model (DEM) for each concerned year. In line with Yang et al. (2011) and Zhu et al. (2016), a rectangle domain covering the seaward part of the mouth bar area and adjacent subaqueous delta is chosen for erosion/deposition calculation (Fig. 1b). The North Passage and the dredged navigation channel are excluded from the study area as this study aims at exploring the morphological impacts of training walls on adjacent areas beyond the North Passage. The total area of the domain is 2 223 m^2, and such a large study area ensures the credibility of the results (Yang et al., 2003). The erosion/deposition patterns are obtained by subtracting a later DEM from an earlier one. The net sediment volume changes of the study area are calculated by summing the product of bed-level change of each grid cell and the cell area. Dividing the net volumes by the time intervals (3–11 years) yields the yearly values, which are compared to assess the morphological processes.

4. Results

4.1. Modeling the hydrodynamics and sediment transport

Modeled hourly flow vectors of a full tidal cycle (13 h) during spring tide in the wet season of 2002 are superposed to represent the flow patterns (Fig. 2). The results indicate that the hydrodynamic fields with and without the training walls show characteristic differences. One of the most remarkable changes is that the flow pattern within the North Passage changed from rotating to reciprocating after the completion of the training walls, and that the currents in groyne-sheltered areas were significantly attenuated. This has also been identified by a previous model-based study (Hu and Ding, 2009). Moreover, the tidal currents at seaward sides of the EHS and Jiuduansha Shoal (JDS) also converts from rotating to reciprocating with decreased flow velocity, implying that the training walls induce weaker tidal currents and longer tidal slack periods at the EHS and JDS. Flow pattern at the adjacent subaqueous delta remains almost unchanged, whereas the flow velocity is slightly enhanced, particularly at the seaward end of the South and North Passage.

Bed shear stress due to tidal currents and waves is an important indicator for estuarine sediment dynamics and subsequent erosion/deposition processes (Zhu et al., 2014). As shown in Fig. 3, the spatial differences of the modeled bed shear stress between model runs illustrate the impacts of training walls. At the flood maximum, the training walls induce the increase in the bed shear stress at the seaward end of the North and South Passage (Fig. 3a). Bed shear stress at the entrance of the South Passage is also increased by the training walls, and this may partly explain the erosion at this area after 1997 (Luan et al., 2016). Meanwhile, the EHS shows decrease in bed shear stress at both flood and ebb maximum (Fig. 3a and b), which is identical with the decreased flow velocity. Bed shear stress within the North Passage shows significant changes, including the decrease in the groyne-sheltered areas and increase in the main channel, particularly during ebb tides (Fig. 3b). Two numerical experiments on the seaward half of the training walls provide more evidences of their impacts. The results indicate that the seaward half of northern training walls increases the bed shear stress at a limited area of the adjacent subaqueous delta during flood tides (Fig. 3c). Notably, bed shear stress at the EHS is decreased

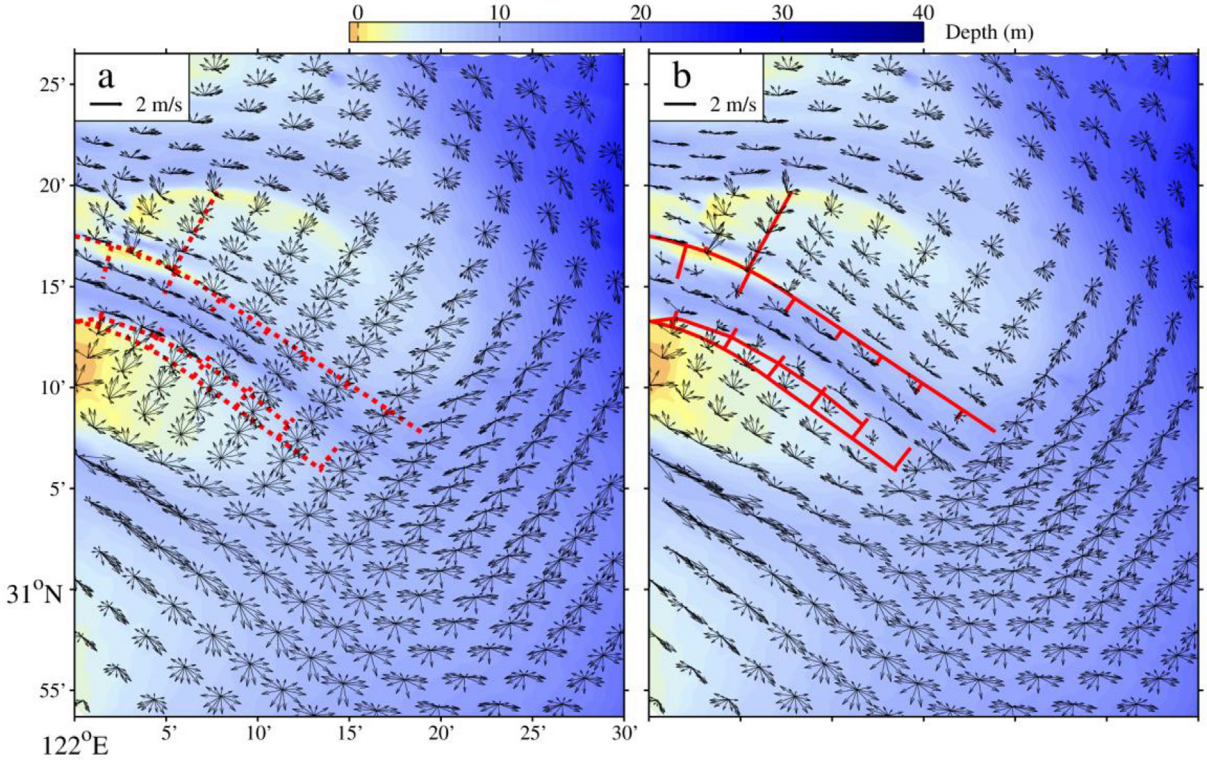

Fig. 2. Superposition of flow vectors of 13 h during spring tide in the wet season of 2002: (a) without training walls; (b) with training walls. The background colors denote the bathymetry of 2002 referred to mean sea-level. (For interpretation of the references to color in this figure legend, the reader is referred to the Web version of this article.)

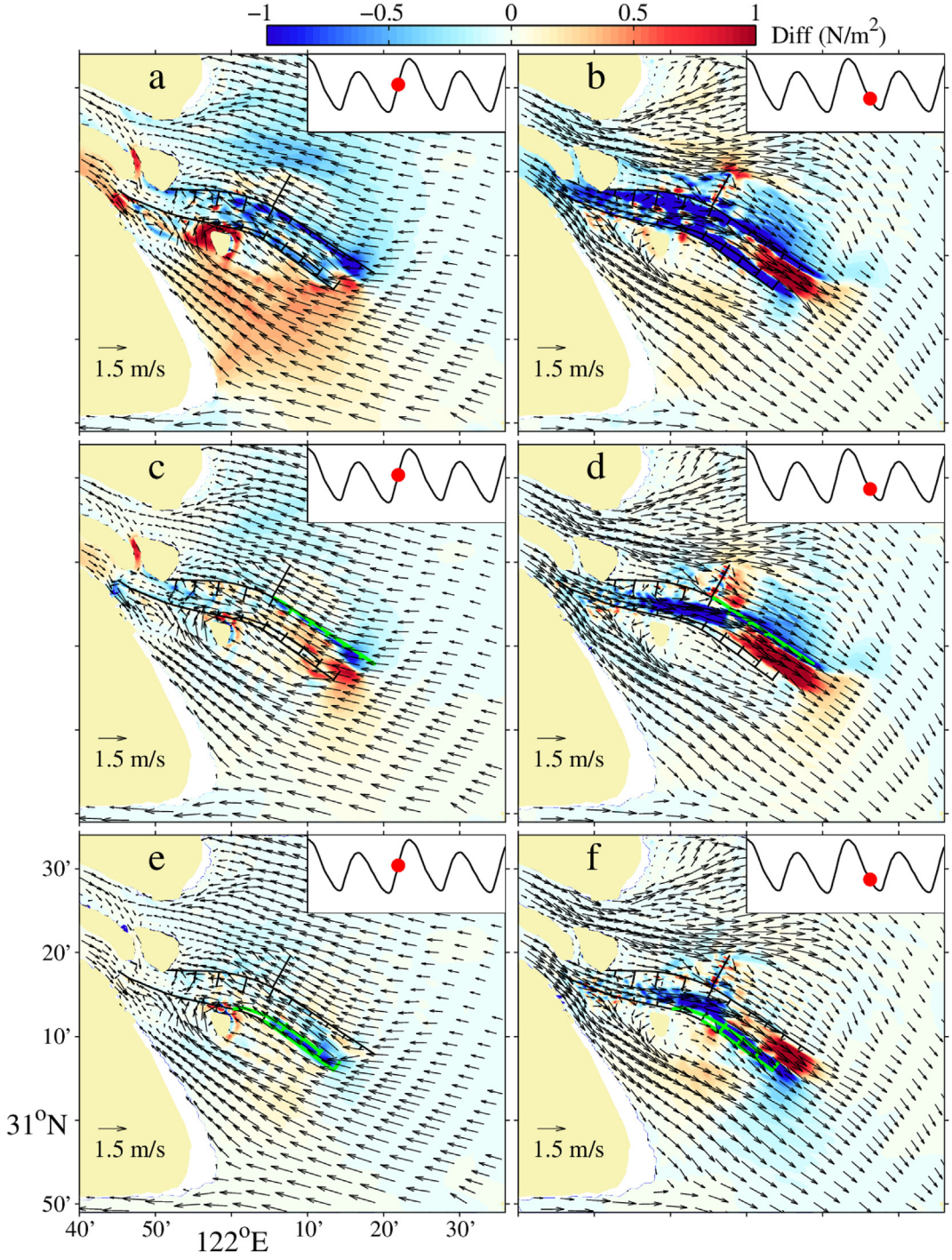

Fig. 3. Tidal currents (arrows) and differences of bed shear stress (background colors) between model runs during spring tide in the wet season of 2002: (a) with and without all training walls at flood maximum; (b) with and without all training walls at ebb maximum; (c) with and without the seaward half of the northern training walls at flood maximum; (d) with and without the seaward half of the northern training walls at ebb maximum; (e) with and without the seaward half of the southern training walls at flood maximum; (f) with and without the seaward half of the southern training walls at ebb maximum (in green color). (For interpretation of the references to color in this figure legend, the reader is referred to the Web version of this article.)

during ebb tides (Fig. 3d), which is consistent with the impacts of all training walls. However, these features are absent in the numerical experiment on the seaward half of southern training walls, and the bed shear stress at the subaqueous delta is even slightly decreased (Fig. 3e and f). Both numerical experiments show significant impacts within the North Passage at ebb maximum, including smaller shear stress at the upper channel and larger at the lower channel (Fig. 3d, f).

In general, the gradient of the residual sediment transport is responsible for bed-level change (Guo et al., 2014). Monthly-averaged sediment flux in the wet season of 2002 with and without the training walls are shown in Fig. 4. Sediment flux along the North Channel and North Passage is significant in the ebb direction in both model runs, and the training walls enhance the flux in the North Passage, suggesting erosion along the main channel. The EHS is fed by sediment from the North Passage across the north dike. Sediment from the North Channel reaches the subaqueous delta and is partly delivered towards the EHS by flood currents. The positive gradient of residual sediment transport from the North Passage to the EHS is significantly increased when the

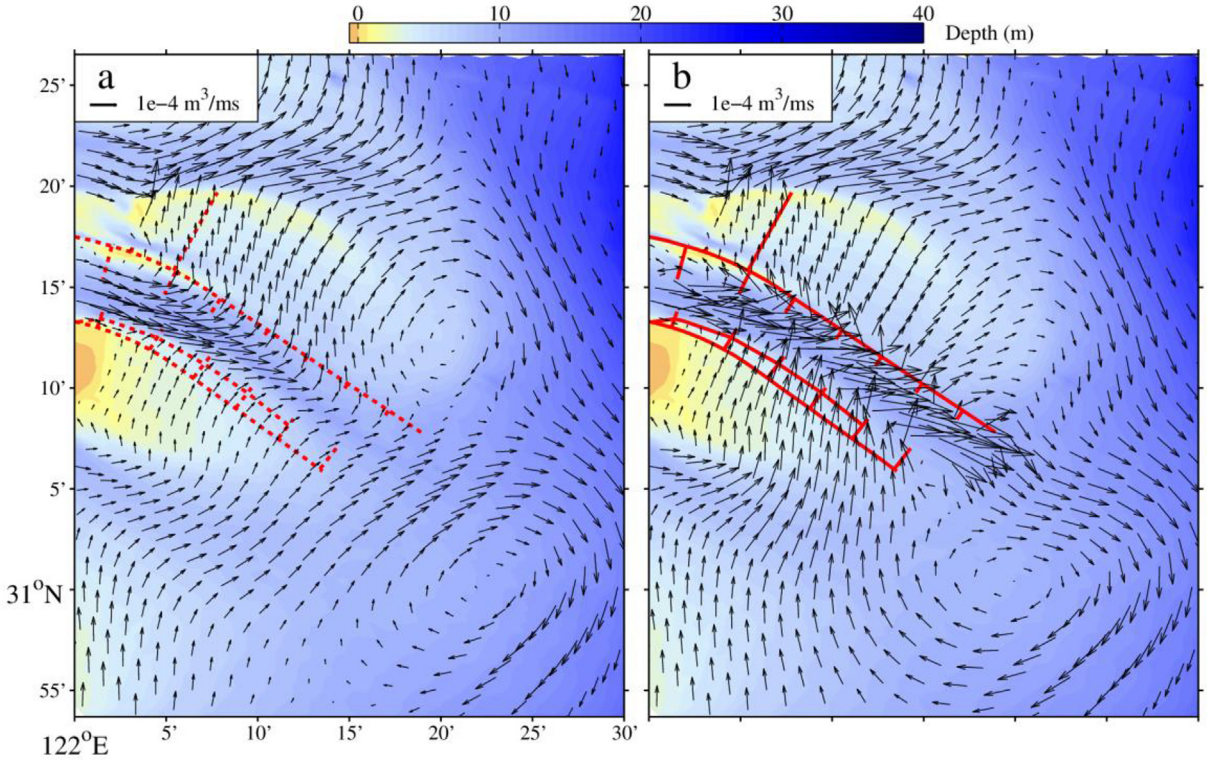

Fig. 4. Monthly-averaged sediment flux in the wet season of 2002: (a) without training walls; (b) with training walls. The background colors denote the bathymetry of 2002 referred to mean sea-level. (For interpretation of the references to color in this figure legend, the reader is referred to the Web version of this article.)

training walls are taken into account. This implies that accretion at the EHS was enhanced after the completion of the DNCP. Meanwhile, the training walls enhance the negative gradient of residual sediment transport at the southern subaqueous delta, suggesting accelerated erosion. The eroded sediment from the subaqueous delta is transported across the south dike and enter the North Passage through a circulation system (Fig. 4b).

4.2. Modeling the morphological changes

The modeled morphological changes under different configurations of the training walls provide direct evidence for the morphological impacts of the DNCP (Fig. 5). The modeled and observed bed-level changes show qualitative agreement as described by Luan et al. (2017). Specifically, the accretion at the EHS and erosion at the subaqueous delta are reproduced with relatively high accuracy (Fig. 5a and b). The promising performance of the hindcast simulation supports it as a reference case for investigating the morphological impacts of the DNCP. The difference between modeled morphological changes with and without the training walls is remarkable within the North Passage, including strong accretion within the groyne-sheltered areas and erosion along the main channel (Fig. 5c). Notably, the model run with training walls produces more accretion at the EHS and stronger erosion at the seaward end of the North and South Passage. This is consistent with the model results of hydrodynamics and sediment transport. Modeling the impact of the seaward half of the northern training walls produces similar results, i.e. enhanced accretion at the EHS and erosion at the subaqueous delta, suggesting the importance of the northern training wall on the morphological patterns (Fig. 5d). Numerical experiment on the seaward half of the southern training walls indicates that the above features are less relevant with the southern training walls. The subaqueous delta near the outlet of the North Passage even shows more accretion (Fig. 5e). In both numerical experiments, the seaward half of the training walls enhance erosion along the main channel of the North Passage.

4.3. Observed morphological changes

Based on bathymetric data analysis, the observed morphological changes indicate that the seaward part of the mouth bar area involved overall accretion in 1986–1997 (Fig. 6a). Both erosion and accretion occurred in the landward part, indicating shoal accretion and channel shifting. The evolution pattern in this period was mainly controlled by natural evolution as higher river sediment discharge fed the delta. The erosion/deposition pattern in 1997–2013 shows distinct spatial variations, reflected by accretion at the EHS and erosion at the adjacent subaqueous delta (Fig. 6b). Two erosion zones formed at the northern ($>$ 10m) and southern (5–10m) subaqueous delta, respectively. The EHS experienced increased accretion from 1986-1997 to 1997–2013 under decreasing river sediment supply. Construction of training walls along the North Passage caused severe deposition in groyne-sheltered areas and erosion at the entrance of the South Passage, while intensive dredging resulted in remarkable deepening along the navigation channel (Luan et al., 2016).

Sediment volume changes showed that the study area converted from net accretion to net erosion along with the decreasing sediment load during 1986–2013 (Fig. 6c). Specifically, the sediment discharge decreased from $314\,\mathrm{Mt\,yr^{-1}}$ in 1997–2002 to $134\,\mathrm{Mt\,yr^{-1}}$ in 2010–2013, and the net volume change presented almost linear decrease from $63.6\,\mathrm{Mm^3\,yr^{-1}}$ in 1997–2002 to $-159.6\,\mathrm{Mm^3\,yr^{-1}}$ in 2010–2013. It is suggested that the river sediment supply was the controlling factor of the overall evolution pattern at a decadal timescale.

In order to investigate the spatial differences of the morphological changes, the study area are firstly divided into a northern part and a southern part by an eastward extending line of the north dike. The 10m-isobath in 1997 is used to further separate the two parts into four subareas in total, i.e. Areas N1, N2, S1 and S2 (Fig. 6a). Four sub-areas

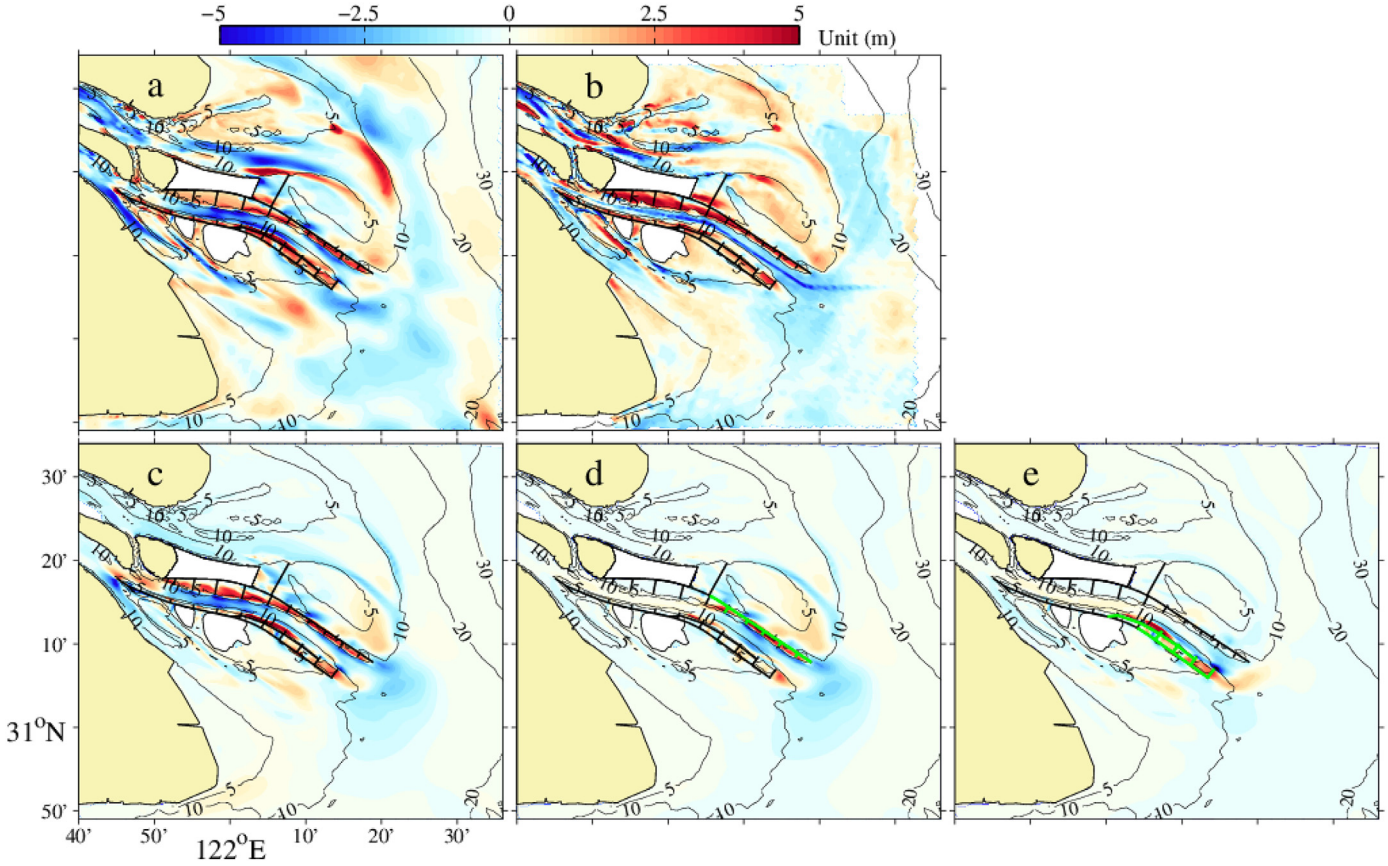

Fig. 5. Modeled (a) and observed (b) erosion/deposition patterns in 2002–2010, and the erosion/deposition differences between model runs with and without all training walls (c), the seaward half of the northern training walls (d) and the seaward half of the southern training walls (e) (in green color). Contours denote the isobaths in 2010 referred to mean sea-level. (For interpretation of the references to color in this figure legend, the reader is referred to the Web version of this article.)

showed various morphological behaviors compared with the entire area in terms of sediment volume changes (Fig. 6d). All the sub-areas were under net accretion in 1986–1997, whereas they involved alternate net accretion and erosion in the subsequent four periods from 1997 to 2013. The Area N1, mainly covering the EHS, experienced net accretion in the first three periods and net erosion in the latest one. The net accretion volume peaked in 2002–2007 (52.7 $Mm^3\,yr^{-1}$). The Area N2, representing the northern erosion zone, involved high accretion amount in 1997–2002 (68.6 $Mm^3\,yr^{-1}$) and altered into continuous erosion after 2002. Net erosion volume in 2002–2007 is higher than that in 2007–2010, and is the highest in 2010–2013. The Area S1, representing the southern erosion zone, underwent increasing erosion since 1997 except the slightly decreased erosion rate in 2010–2013. The accumulated net volume change of the Area N2 from 2002 to 2013 was −555 Mm^3, while the value of the Area S1 from 1997 to 2013 was −523 Mm^3. The Area S2 converted from net accretion to net erosion around the year 2007, and the erosion amount after 2007 is relatively low suggesting slow morphological changes in this area. Notably, all the sub-areas showed net erosion in 2010–2013, indicating that the subaqueous delta had undergone overall erosion in recent years.

5. Discussion

5.1. Conversion from accretion to erosion due to river sediment reduction

The Yangtze mouth bar area and subaqueous delta was estimated to accumulate over 40% of the fluvial sediment in the past millennia (Milliman et al., 1985; Liu et al., 2007), resulting in nearly 50 m of modern sediment layer in the seabed (Stanley and Chen, 1993). This muddy area is the depocenter of the Yangtze River delta, which is also regarded as the turbidity maxima due to frequent near-bottom sediment exchange (Liu et al., 2010). As the sediment load started to decline in the 1980s, the net accretion amount deceased from 40.6 $Mm^3\,yr^{-1}$ in 1986–1997 to 8.1 $Mm^3\,yr^{-1}$ in 2002–2007 to retain high suspended sediment concentration (SSC) in the mouth bar area. Once the sediment load dropped below a critical level (Yang et al., 2003), abundant bed sediment turned to compensate the decreased SSC by erosion. Thus, there is a time lag between the decreases in sediment discharge and SSC (Li et al., 2012). Along with the continuous decrease in sediment discharge, both erosion of the subaqueous delta and the decrease in SSC was initiated. The net erosion amount of the study area was −60.7 $Mt\,yr^{-1}$ in 2007–2010 and −159.6 $Mt\,yr^{-1}$ in 2010–2013. Based on the statistical analysis of measurements, Li et al. (2012) found that the mean surface SSC at the subaqueous delta has decreased by 20–30% over the past 10–20 years. Li et al. (2012) also reported that the mean surface SSC in the north of the subaqueous delta showed much lower decrease rate (e.g., 5% at Sheshan Station) than the south (e.g., 30% at Dajishan Station). This suggests that more bed sediment in the north is resuspended to partly offset the SSC decrease, and may explain more erosion in the Area N2 than the Area S1. Generally, delta progradation or regression depends on the sediment budget between fluvial supply and offshore dispersal (Syvitski and Saito, 2007; Canestrelli et al., 2010). Under decreasing river sediment supply and relatively stable dispersal amount by coastal currents (Deng et al., 2017), the conversion from accretion to erosion of Yangtze subaqueous delta seems to be an inevitable tendency.

5.2. Distinct morphodynamic features due to the DNCP

According to the overall evolution pattern, morphodynamics of the

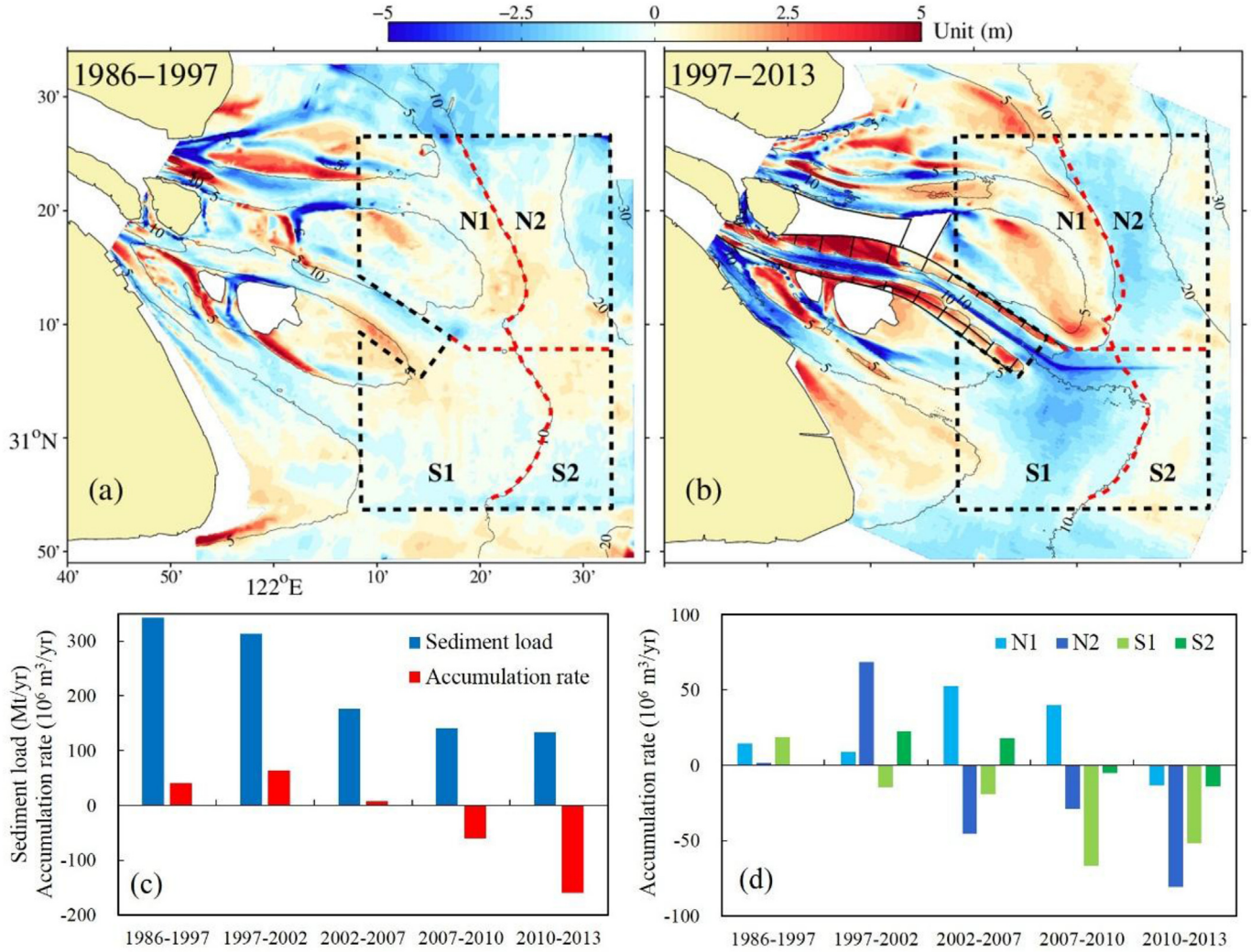

Fig. 6. (a) Erosion/deposition pattern in 1986–1997; (b) erosion/deposition pattern in 1997–2013; (c) annual-mean sediment load at Datong station and accumulation rate of the entire study area; (d) accumulation rate of four sub-areas. The dredged navigation channel is excluded in the calculations of volume change. The entire study area surrounded by black dashed lines is divided by red dashed lines into four sub-areas in (a) and (b). The isobaths in the latter year are presented. (For interpretation of the references to color in this figure legend, the reader is referred to the Web version of this article.)

Yangtze River delta show distinct spatiotemporal variations during 1997–2013. One remarkable feature is the enhanced accretion at the EHS (Fig. 6b), which is conflicting with the evolution trend of the entire study area under river sediment reduction. As indicated by the model results, the reciprocating flow pattern with weaker tidal current and longer slack period features the EHS as a depositional environment after the construction of training walls. The suspended sediment transported by flood currents tended to settle and accumulate at the EHS. Thus, the EHS converted to a sediment-starved status after the DNCP. This can explain the observed accretion peak of the EHS in 2002–2007, during which the dikes were extended to the present location in Phase II (Fig. 1c). It can be concluded that the enhanced accretion at the EHS was caused by the training walls along the North Passage, particularly the seaward half of the northern training walls, which significantly modified the hydrodynamic fields and sediment transport processes at the EHS.

Another evolution feature is the formation of two erosion zones at the subaqueous delta (Fig. 6b). Locations of both erosion zones are estuarine muddy areas where the seabed is mainly composed of unconsolidated fine-grained sediment (Fig. 7). Under combined river and tidal forcing, these muddy areas are subject to intensive sediment exchange between the water column and seabed through deposition and resuspension (Liu et al., 2010). Bed level changes of these areas are more sensitive to variations of the SSC and hydrodynamic condition than areas covered by coarser sediment (Luan et al., 2016). Assuming that no training walls were constructed along the North Passage, erosion at the subaqueous delta is probably inevitable due to river sediment reduction. Model results demonstrate that the training walls enhanced the bed shear stress at the southern erosion zone, and subsequently accelerated erosion of the subaqueous delta.

The Yangtze River delta has been heavily interfered by both river sediment reduction and large-scale estuarine engineering projects in recent decades, resulting in complicated morphological evolution patterns within the delta (Yang et al., 2011; Dai et al., 2014; Luan et al., 2016; Luo et al., 2017). River sediment reduction has triggered erosion of the subaqueous delta (Fig. 6c). The large-scale DNCP caused significant morphological changes within the North Passage (Dai et al., 2013) and adjacent area (this study). Due to the construction of training walls, the North Passage experienced net accretion of 17.2 Mm^3/yr in 1998–2011 though the navigation channel was deepened by dredging (Dai et al., 2013). The annual dredging volume was 47.2 Mm^3/yr in 2000–2012 (Luan et al., 2016), and a considerable portion of the dredged sediment was used for siltation promotion and land reclamation at the EHS. Wei et al. (2017) reported that annual accretion volume at East Nanhui Mudflat reached 12 Mm^3/yr in 1998–2013. Meanwhile, the annual accretion volume at the EHS is 47.9 Mm^3/yr in 2002–2010.

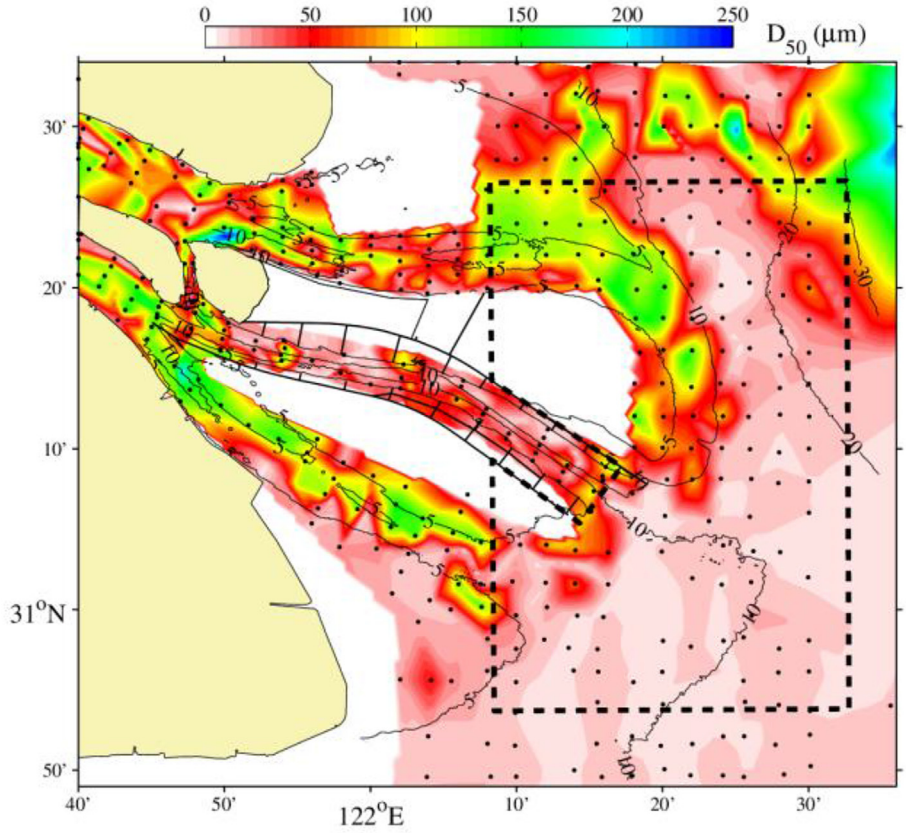

Fig. 7. Median grain size (D_{50}) at the Yangtze mouth bar area and adjacent subaqueous delta (black dots denote bed surface sediment samples in September 2015, and dashed line denotes the boundary of the study area as shown in Fig. 1b).

The above sediment accretion is the important contributor for the mouth bar area to retain net accretion since 1997 under low river sediment supply (Luan et al., 2016). The summation of the accretion amounts is as large as > 150 Mt/yr (dry bulk density of the sediment 1.22 t/m^3) though the calculation periods are slightly different. Annual mean sediment discharge in 1997–2013 is 203 Mt/yr, which is lower than the transport capacity of the coastal current estimated through observation (270 Mt/yr). Milliman et al. (1985) estimated the southward dispersal amount of river sediment load is about 150 Mt/yr. To close the sediment budget, it is essential to take sediment eroded from the subaqueous delta into account. Model results suggest that training walls enhanced the scouring capacity of tidal currents at the subaqueous delta and thereby accelerated the erosion at this muddy area. Eroded sediment is transported to the North Passage by flood currents (Fig. 4b), and is likely to fill in the navigation channel. Continuous dredging activities along the navigation could facilitate the back-siltation, which may indirectly increase the net erosion of the subaqueous delta. Based on the analysis on the overall sediment budget of the Yangtze River delta, the morphological impacts of the DNCP are separated from decreasing river sediment load. Moreover, the physical mechanism is also revealed in terms of hydrodynamics and sediment transport, applying process-based modelling approach and bathymetry date analysis.

Based on the observed morphological evolution patterns and process-based modeling results, the sediment transport paths and erosion/deposition patterns before and after the DNCP are schematized as shown in the Fig. 8. Before the DNCP, the north part of the subaqueous delta was under accretion with stronger accretion at the mouth of the North Channel than the EHS, while slight erosion has occurred at the seaward end of the North and South Passage (Fig. 8a). The eroded sediment was involved in a circulation system and was partly delivered to the outer sea by tidal currents. After the north dike was extended to its present location, suspended sediment driven by tidal currents tends to deposit at the EHS, resulting in enhanced accretion (Fig. 8b). Meanwhile, the mouth of the North Channel converted from accretion to strong erosion, forming the northern erosion zone (Fig. 6b). Erosion at the seaward end of the North and South Passage was enhanced by the training walls superimposed upon erosion due to river sediment reduction. The eroded sediment from both erosion zones was partially transported across the south dike and may become an important source for back-siltation of the navigation channel along the North Passage (Zhu et al., 2016), while the rest was dispersed by the alongshore coastal current towards the south. It is suggested that the retained accretion of the mouth bar area in 1997–2010 as described by Luan et al. (2016) largely relied on sediment eroded from the subaqueous delta in addition to fluvial supply. With the conversion from accretion to erosion due to river sediment reduction, the Yangtze River delta showed complicated evolution patterns under large-scale estuarine engineering projects.

5.3. Implications for delta management

The geomorphic functions of the Yangtze River delta have been significantly affected by large-scale estuarine engineering projects. Present study indicates that the DNCP induced strong deposition at local and adjacent sites, including the groyne-sheltered areas, the deep navigation channel (back-siltation) and the EHS. Moreover, it is reported that the dredging materials along the navigation channel provided a considerable amount of sediment for land reclamation at the EHS. According to the schematized paths of sediment transport after the DNCP (Fig. 8b), siltation promoting projects within the mouth bar area could aggravate the erosion at the subaqueous delta through accumulating the eroded sediment for land creation and shallow shoal accretion. The present erosion thickness has not yet reached the maximum

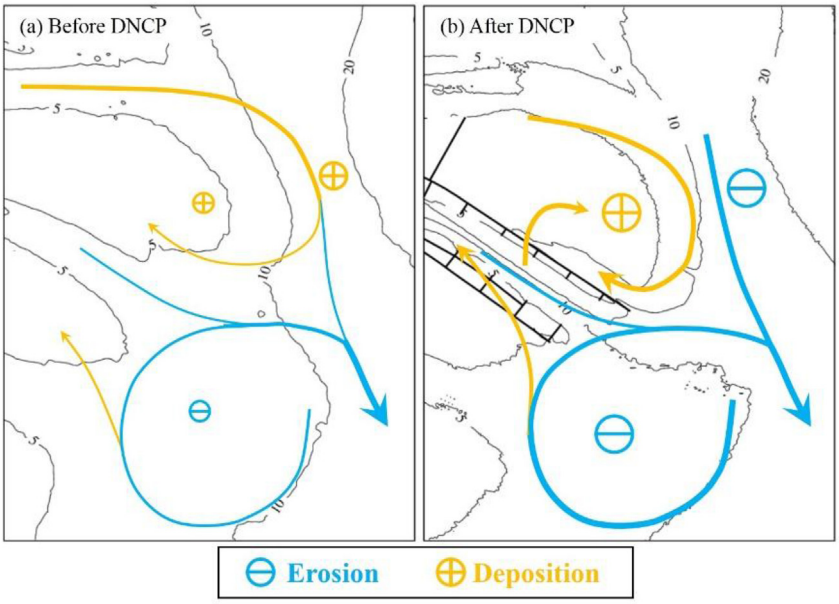

Fig. 8. Schematized paths of sediment transport (arrows) and erosion/deposition patterns at the Yangtze subaqueous delta before (a) and after (b) the DNCP.

(Yang et al., 2017), suggesting that deepening is likely to continue in the future. Continuous erosion at the subaqueous delta may cause engineering failures and increase the exposure risk of buried oil/gas pipelines. Close attention on the erosion zones is required for the safety of engineering structures. Besides, the EHS is proposed to build an excavated harbor basin to meet the increasing shipping demand of the Shanghai Harbor (Ding and Li, 2013). Though the dike-induced accretion at the EHS is favorable for the harbor construction, net erosion was observed at the EHS after 2010. Therefore, sustainable management of the Yangtze River delta requires continuous bathymetry measurements and reliable prediction on evolution trend under both continuous river sediment reduction and construction of new engineering projects in the future (Yang et al., 2014). Among the global dataset of river deltas, the Yangtze River delta is a typical example under interactive impacts of large-scale engineering projects in both the watershed and the estuary (Syvitski et al., 2009; Tessler et al., 2015). The responding time of the subaqueous delta to human interventions and its equilibrium status remain unknown and merits further systematic research.

6. Conclusions

This study addresses the morphological impacts of large-scale estuarine engineering projects on the Yangtze River delta in 1997–2013 combining process-based simulations (Delft3D) and bathymetric data analysis. The period 1997–2013 coincides with the construction period of the DNCP along the North Passage (1997–2010). The results reveal that the seaward part of the mouth bar area and adjacent subaqueous delta, defined as the study area, converted from net accretion to net erosion, primarily caused by river sediment reduction. The erosion/deposition pattern of the study area show strong spatial variations in 1997–2013. Two erosion zones formed at the mouth of the North Channel and the seaward end of the North and South Passage, respectively. The EHS involved abnormal accretion under decreasing sediment discharge, and the accretion peaked in 2002–2007. Process-based modeling approach (Delft3D) is applied to investigate the impacts of the training walls. Hydrodynamic simulations indicate that the training walls change the flow pattern at the EHS from rotating to reciprocating with decreased flow velocity, particularly with decreased bed shear stress during ebb tide. Longer tidal slack period and weaker hydrodynamic condition characterize the EHS as a zone of sediment starvation. The flow pattern at the southern erosion zone shows no evident change after the DNCP, whereas the currents are enhanced as reflected by larger bed shear stress during rising tides. Morphological modeling results show that the training walls enhanced the accretion at the EHS and erosion at the southern erosion zone, and these impacts are primarily contributed by the seaward half of the north dike. This can explain the accretion peak of the EHS in 2002–2007, during which the seaward halves of the twin dikes were constructed in Phase II (2002–2005). The schematized sediment transport paths after the DNCP indicate that siltation promoting projects within the mouth bar area increased shallow shoal accretion and aggravated erosion at the subaqueous delta. Overall, these results can be beneficial to sustainable management of the Yangtze River delta and other similar large river deltas under diminishing river sediment supplies and local human interventions.

Acknowledgments

This paper is a product of the project “Coping with deltas in transition” within the Programme of Strategic Scientific Alliances between China and The Netherlands (PSA), financed by the Chinese Ministry of Science and Technology (MOST), Project no. 2016YFE0133700 and Royal Netherlands Academy of Arts and Sciences (KNAW), Project no. PSA-SA-E-02. This study was also financed by the Ministry of Science and Technology of China (2016YFA0600903), the Key Project of the Shanghai Science & Technology Committee in China (17DJ14003) and the National Natural Science Foundation of China (51339001 and 51679010). The bathymetry data used in this study are gratefully provided by Navigation Guarantee Department of the Chinese Navy Headquarters, Shanghai Waterway Bureau of Ministry of Transport and Yangtze Estuary Waterway Administration Bureau of Ministry of Transport. The authors are grateful to Prof. Inigo Losada (Editor-in-Chief) and two anonymous reviewers for their thoughtful and constructive comments and suggestions.

References

Anthony, E.J., Brunier, G., Besset, M., Goichot, M., Dussouillez, P., Nguyen, V.L., 2015. Linking rapid erosion of the Mekong River delta to human activities. Sci. Rep-Uk 5, 14745.

Blott, S.J., Pye, K., van der Wal, D., Neal, A., 2006. Long-term morphological change and its causes in the Mersey estuary, NW England. Geomorphology 81, 185–206.

Blum, M.D., Roberts, H.H., 2009. Drowning of the Mississippi Delta due to insufficient sediment supply and global sea-level rise. Nat. Geosci. 2, 488–491.
Canestrelli, A., Fagherazzi, S., Defina, A., Lanzoni, S., 2010. Tidal hydrodynamics and erosional power in the Fly River delta, Papua New Guinea. J. Geophys. Res.: Earth Surface 115, F4033.
Chen, J., Zhu, H., Dong, Y., Sun, J., 1985. Development of the Changjiang estuary and its submerged delta. Continent. Shelf Res. 4, 47–56.
Chu, Z.X., Sun, X.G., Zhai, S.K., Xu, K.H., 2006. Changing pattern of accretion/erosion of the modern Yellow River (Huanghe) subaerial delta, China: based on remote sensing images. Mar. Geol. 227, 13–30.
Coleman, J.M., Wright, L.D., 1975. Modern river deltas: variability of processes and sand bodies. In: Broussard, M.L. (Ed.), Deltas: Models for Exploration. Houston Geological Society, pp. 99–149.
Dai, Z., Liu, J.T., Fu, G., Xie, H., 2013. A thirteen-year record of bathymetric changes in the North Passage, Changjiang (Yangtze) estuary. Geomorphology 187, 101–107.
Dai, Z., Liu, J.T., Wei, W., Chen, J., 2014. Detection of the three gorges dam influence on the Changjiang (Yangtze River) submerged delta. Sci Rep-Uk 4, 6600.
Day, J., Hall, C.S., Kemp, W.M., Yanez-Arancibia, A., 1989. Estuarine Ecology. John-Wiley, New York.
de Vet, P.L.M., van Prooijen, B.C., Wang, Z.B., 2017. The differences in morphological development between the intertidal flats of the Eastern and Western Scheldt. Geomorphology 281, 31–42.
De Vriend, H., Wang, Z., Ysebaert, T., Herman, P.J., Ding, P., 2011. Eco-morphological problems in the Yangtze estuary and the western Scheldt. Wetlands 31, 1033–1042.
Deltares, 2014. User Manual Delft3D-flow: Simulation of Multi-dimensional Hydrodynamic Flows and Transport Phenomena, Including Sediments. Version 3.15, Delft, Netherlands.
Deng, B., Wu, H., Yang, S., Zhang, J., 2017. Longshore suspended sediment transport and its implications for submarine erosion off the Yangtze River Estuary. Estuar. Coast Shelf Sci. 190, 1–10.
Ding, P.X., Li, S.G., 2013. Planning ideas and key technology for building excavated-in harbor basin in the Hengsha Shoal of the Yangtze Estuary. J. East China Normal Univ. (Nat. Sci.) 1–9.
Dissanayake, D.M.P.K., Wurpts, A., Miani, M., Knaack, H., Niemeyer, H.D., Roelvink, J.A., 2012. Modelling morphodynamic response of a tidal basin to an anthropogenic effect: ley Bay, East Frisian Wadden Sea-applying tidal forcing only and different sediment fractions. Coast Eng. 67, 14–28.
Eelkema, M., Wang, Z.B., Hibma, A., Stive, M.J., 2013. Morphological effects of the Eastern Scheldt storm surge barrier on the ebb-tidal delta. Coast Eng. J. 55, 1350010.
Galloway, W.E., 1975. Process framework for describing the morphologic and stratigraphic evolution of deltaic depositional systems. In: Broussard, M.L. (Ed.), Deltas: Models for Exploration. Houston Geological Society, pp. 87–98.
Ge, C., Zhang, W., Dong, C., Wang, F., Feng, H., Qu, J., Yu, L., 2017. Tracing sediment erosion in the Yangtze River subaqueous delta using magnetic methods. J. Geophys. Res.: Earth Surface 122, 2064–2078.
Ge, J., Ding, P., Chen, C., Hu, S., Fu, G., Wu, L., 2013. An integrated East China Sea–Changjiang Estuary model system with aim at resolving multi-scale regional—shelf–estuarine dynamics. Ocean Dynam. 63, 881–900.
Guo, L., van der Wegen, M., Roelvink, J.A., He, Q., 2014. The role of river flow and tidal asymmetry on 1D estuarine morphodynamics. J. Geophys. Res.: Earth Surface 119.
Hu, K., Ding, P., 2009. The effect of deep Waterway constructions on hydrodynamics and salinities in Yangtze estuary, China. J. Coast Res. 961–965.
Lesser, G.R., Roelvink, J.A., van Kester, J.A.T.M., Stelling, G.S., 2004. Development and validation of a three-dimensional morphological model. Coast Eng. 51, 883–915.
Li, P., Yang, S.L., Milliman, J.D., Xu, K.H., Qin, W.H., Wu, C.S., Chen, Y.P., Shi, B.W., 2012. Spatial, temporal, and human-induced variations in suspended sediment concentration in the surface waters of the Yangtze estuary and adjacent coastal areas. Estuar. Coast 35, 1316–1327.
Li, X., Liu, J.P., Tian, B., 2016. Evolution of the Jiuduansha wetland and the impact of navigation works in the Yangtze Estuary, China. Geomorphology 253, 328–339.
Liu, G., Zhu, J., Wang, Y., Wu, H., Wu, J., 2011. Tripod measured residual currents and sediment flux: impacts on the silting of the deepwater navigation channel in the Changjiang estuary. Estuar. Coast Shelf Sci. 93, 192–201.
Liu, H., He, Q., Wang, Z., Weltje, G.J., Zhang, J., 2010. Dynamics and spatial variability of near-bottom sediment exchange in the Yangtze Estuary, China. Estuar. Coast Shelf Sci. 86, 322–330.
Liu, J.P., Xu, K.H., Li, A.C., Milliman, J.D., Velozzi, D.M., Xiao, S.B., Yang, Z.S., 2007. Flux and fate of Yangtze River sediment delivered to the East China sea. Geomorphology 85, 208–224.
Luan, H.L., Ding, P.X., Wang, Z.B., Ge, J.Z., 2017. Process-based morphodynamic modeling of the Yangtze Estuary at a decadal timescale: controls on estuarine evolution and future trends. Geomorphology 290, 347–364.
Luan, H.L., Ding, P.X., Wang, Z.B., Ge, J.Z., Yang, S.L., 2016. Decadal morphological evolution of the Yangtze Estuary in response to river input changes and estuarine engineering projects. Geomorphology 265, 12–23.
Luo, X.X., Yang, S.L., Wang, R.S., Zhang, C.Y., Li, P., 2017. New evidence of Yangtze delta recession after closing of the three gorges dam. Sci Rep-Uk 7.
Luo, X.X., Yang, S.L., Zhang, J., 2012. The impact of the Three Gorges Dam on the downstream distribution and texture of sediments along the middle and lower Yangtze River (Changjiang) and its estuary, and subsequent sediment dispersal in the East China Sea. Geomorphology 179, 126–140.
Milliman, J.D., Farnsworth, K.L., 2011. River Discharge to the Coastal Ocean: a Global Synthesis. Cambridge University Press, Cambridge.
Milliman, J.D., Shen, H.T., Yang, Z.S., Mead, R.H., 1985. Transport and deposition of river sediment in the Changjiang estuary and adjacent continental shelf. Continent. Shelf Res. 4, 37–45.
Morton, R.A., Bernier, J.C., Barras, J.A., Ferina, N.F., 2005. Rapid Subsidence and Historical Wetland Loss in the Mississippi Delta Plain: Likely Causes and Future Implications. US Geol. Surv., Washington, DC.
Roelvink, J.A., 2006. Coastal morphodynamic evolution techniques. Coast Eng. 53, 277–287.
Sanchez-Arcilla, A., Jimenez, J.A., Valdemoro, H.I., 1998. The Ebro delta: morphodynamics and vulnerability. J. Coast Res. 14, 755–772.
Stanley, D.J., 1996. Nile delta: extreme case of sediment entrapment on a delta plain and consequent coastal land loss. Mar. Geol. 129, 189–195.
Stanley, D.J., Chen, Z., 1993. Yangtze delta, eastern China: 1. Geometry and subsidence of Holocene depocenter. Mar. Geol. 112, 1–11.
Stanley, D.J., Warne, A.G., 1994. Worldwide initiation of Holocene marine deltas by deceleration of sea-level rise. Science 265, 228–231.
Su, M., Yao, P., Wang, Z.B., Zhang, C.K., Stive, M.J.F., 2016. Exploratory morphodynamic hindcast of the evolution of the abandoned Yellow River delta, 1578-1855 AD. Mar. Geol. 383, 99–119.
Syvitski, J.P.M., 2008. Deltas at risk. Sustain Sci 3, 23–32.
Syvitski, J.P.M., Kettner, A.J., Overeem, I., Hutton, E.W.H., Hannon, M.T., Brakenridge, G.R., Day, J., Vorosmarty, C., Saito, Y., Giosan, L., Nicholls, R.J., 2009. Sinking deltas due to human activities. Nat. Geosci. 2, 681–686.
Syvitski, J.P.M., Saito, Y., 2007. Morphodynamics of deltas under the influence of humans. Global Planet. Change 57, 261–282.
Tessler, Z.D., Vörösmarty, C.J., Grossberg, M., Gladkova, I., Aizenman, H., Syvitski, J.P.M., Foufoula-Georgiou, E., 2015. Profiling risk and sustainability in coastal deltas of the world. Science 349, 638–643.
Thomas, C.G., Spearman, J.R., Turnbull, M.J., 2002. Historical morphological change in the Mersey estuary. Continent. Shelf Res. 22, 1775–1794.
Tian, B., Zhou, Y., Thom, R.M., Diefenderfer, H.L., Yuan, Q., 2015. Detecting wetland changes in Shanghai, China using FORMOSAT and Landsat TM imagery. J. Hydrol. 529, 1–10.
van der Wegen, M., Jaffe, B.E., Roelvink, J.A., 2011. Process-based, morphodynamic hindcast of decadal deposition patterns in San Pablo Bay, California, 1856–1887. J. Geophys. Res. Earth Surface 116, F2008.
van Maren, D.S., van Kessel, T., Cronin, K., Sittoni, L., 2015. The impact of channel deepening and dredging on estuarine sediment concentration. Continent. Shelf Res. 95, 1–14.
Wang, H., Yang, Z., Saito, Y., Liu, J.P., Sun, X., Wang, Y., 2007. Stepwise decreases of the Huanghe (Yellow River) sediment load (1950–2005): impacts of climate change and human activities. Global Planet. Change 57, 331–354.
Wang, J., Baskaran, M., Hou, X., Du, J., Zhang, J., 2017. Historical changes in 239Pu and 240Pu sources in sedimentary records in the East China Sea: implications for provenance and transportation. Earth Planet Sci. Lett. 466, 32–42.
Wang, Z.B., Van Maren, D.S., Ding, P.X., Yang, S.L., Van Prooijen, B.C., De Vet, P.L.M., Winterwerp, J.C., De Vriend, H.J., Stive, M.J.F., He, Q., 2015. Human impacts on morphodynamic thresholds in estuarine systems. Continent. Shelf Res., R3681.
Wei, W., Tang, Z., Dai, Z., Lin, Y., Ge, Z., Gao, J., 2015. Variations in tidal flats of the Changjiang (Yangtze) estuary during 1950s–2010s: future crisis and policy implication. Ocean Coast Manag. 108, 89–96.
Wei, W., Mei, X., Dai, Z., Tang, Z., 2016. Recent morphodynamic evolution of the largest uninhibited island in the Yangtze (Changjiang) estuary during 1998–2014: influence of the anthropogenic interference. Continent. Shelf Res. 124, 83–94.
Wei, W., Dai, Z., Mei, X., Liu, J.P., Gao, S., Li, S., 2017. Shoal morphodynamics of the Changjiang (Yangtze) estuary: influences from river damming, estuarine hydraulic engineering and reclamation projects. Mar. Geol. 386, 32–43.
Wu, Z.Y., Saito, Y., Zhao, D.N., Zhou, J.Q., Cao, Z.Y., Li, S.J., Shang, J.H., Liang, Y.Y., 2016. Impact of human activities on subaqueous topographic change in Lingding Bay of the Pearl River estuary, China, during 1955–2013. Sci Rep-Uk 6, 37742.
Yang, H.F., Yang, S.L., Meng, Y., Xu, K.H., Luo, X.X., Wu, C.S., Shi, B.W., 2018. Recent coarsening of sediments on the southern Yangtze subaqueous delta front: a response to river damming. Continent. Shelf Res. 155, 45–51.
Yang, H.F., Yang, S.L., Xu, K.H., Wu, H., Shi, B.W., 2017. Erosion potential of the Yangtze Delta under sediment starvation and climate change. Sci Rep-Uk 7, 10535.
Yang, S.L., Belkin, I.M., Belkina, A.I., Zhao, Q.Y., Zhu, J., Ding, P.X., 2003. Delta response to decline in sediment supply from the Yangtze River: evidence of the recent four decades and expectations for the next half-century. Estuar. Coast Shelf Sci. 57, 689–699.
Yang, S.L., Milliman, J.D., Li, P., Xu, K., 2011. 50,000 dams later: erosion of the Yangtze River and its delta. Global Planet. Change 75, 14–20.
Yang, S.L., Milliman, J.D., Xu, K.H., Deng, B., Zhang, X.Y., Luo, X.X., 2014. Downstream sedimentary and geomorphic impacts of the three gorges dam on the Yangtze River. Earth Sci. Rev. 138, 469–486.
Yang, S.L., Xu, K.H., Milliman, J.D., Yang, H.F., Wu, C.S., 2015. Decline of Yangtze River water and sediment discharge: impact from natural and anthropogenic changes. Sci Rep-Uk 5, 12581.
Yun, C., 2004. Recent Evolution of Yangtze Estuary and its Mechanisms. China Ocean Press, Beijing, China (in Chinese).
Zhu, L., He, Q., Shen, J., Wang, Y., 2016. The influence of human activities on morphodynamics and alteration of sediment source and sink in the Changjiang Estuary. Geomorphology 273, 52–62.
Zhu, Q., Yang, S., Ma, Y., 2014. Intra-tidal sedimentary processes associated with combined wave–current action on an exposed, erosional mudflat, southeastern Yangtze River Delta, China. Mar. Geol. 347, 95–106.